COMPDYN 2019
7th ECCOMAS Thematic Conference on
Computational Methods in Structural Dynamics and Earthquake Engineering
M. Papadrakakis, M. Fragiadakis (eds.)
Crete, Greece, 24–26 June 2019

3D DETAILED MODELING OF REINFORCED CONCRETE FRAMES CONSIDERING ACCUMULATED DAMAGE DURING STATIC CYCLIC AND DYNAMIC ANALYSIS – NEW VALIDATION CASE STUDIES

Christos Mourlas [1], George Markou [2], and Manolis Papadrakakis [1]

[1] Institute of Structural Analysis & Seismic Research, National Technical University of Athens, 9 Iroon Polytechniou Str., Zografou Campus, GR-15780 Athens, Greece
e-mail: {mourlasch, mpapadra}@central.ntua.gr

[2] Department of Civil Engineering, University of Pretoria, South Africa
e-mail: george.markou@up.ac.za

Abstract

The study of the hysteretic behavior of reinforced concrete members that undergo static cyclic and dynamic loading conditions in cases where the loading level is close to their carrying capacity, is a challenging open research subject, which currently is being investigated by many researchers. The development of an objective and robust 3D constitutive modeling approach that will be able to account for the accumulated material damage and stiffness deterioration is of great importance in order to realistically describe the physical failure mechanisms thus numerically study the seismic performance of RC structures. The adopted concrete material model in this research work is based on the material model proposed by Markou and Papadrakakis, which was an extension of the Kotsovos and Pavlovic work. Furthermore, the use of two newly proposed damage factors that are computed through the use of the number of opening and closing of cracks during the nonlinear cyclic analysis, are further investigated and their ability in capturing the accumulated material damage in both steel and concrete is further discussed in this research work.
The numerical accuracy of the proposed method is validated by comparing the numerical results with the experimental data of two beam-column frame joints, a shear wall and a three-storey three-bay RC frame. According to the experimental setups, the RC joint and the shear wall specimens were tested under ultimate limit state cyclic loading, whereas the RC frame was tested under dynamic loading conditions. Based on the numerical findings, the proposed algorithm manages to capture the experimental results in an accurate manner and the numerical response of the understudy algorithmic implementation was found to exhibit computational robustness and efficiency.

Keywords: Nonlinear dynamic analysis, concrete material modeling, finite element method, damage factor, accumulated material damage

1 INTRODUCTION

Many numerical constitutive models have been proposed for the simulation of reinforced concrete (RC) structural members. Most of these approaches are based on uniaxial constitutive laws with strain softening and tension stiffening characteristics. The analysis of RC structural members under ultimate limit state conditions is characterized by heavy nonlinearity, which is mainly caused by the cracking of concrete and steel rapture. Mainly due to the complex behavior of concrete structures under cyclic and dynamic loading conditions, the numerical procedure becomes unstable causing the nonlinear solution procedure to diverge. Therefore, a realistic 3D approach that is characterized by simplicity and computational efficiency is an open research subject for Civil Engineering scientific community.

As a solution to this numerical modeling limitation, most researchers use uniaxial constitutive laws that can describe only certain aspects of concrete behavior. Many of these numerical approaches are based on elastoplasticity theories, thermodynamic laws and fracture mechanics. These models place emphasis on strain softening, tension stiffening characteristics and generally they foresee for numerous material parameters that describe the post cracking behavior of concrete. By adopting this approach, they introduce properties of concrete that are related to the triaxial behavior of concrete such as plasticity, concrete crushing and effect of confinement, but have no actual physical meaning nor interpretation. Additionally, most of these models are restricted to 2D analysis in order to capture the biaxial behavior of concrete structures that are subjected to monotonic loading conditions. This makes these numerical material models difficult to handle (lacking in objectivity) and not of practical interest given their limited applicability. Therefore, the necessity of a 3D constitutive material law that will not require additional material parameters that are not associated with the behavior of concrete at a material level is required.

Furthermore, the implementation of the pre-mentioned modeling methods is limited to examples of small practical interest (i.e. single structural members). Thus, it is important to formulate a constitutive model that will represent accurately the realistic mechanical behavior of concrete and offer the required computational efficiency allowing its implementation in full-scale structure nonlinear dynamic analysis.

The proposed approach described in [1, 2] and further investigated herein, emphasizes on the objectivity and the applicability of the proposed modeling method under nonlinear static cyclic and dynamic analysis of RC structures. In this research article, the proposed damage parameters for concrete and steel reinforcement that are proposed in [2], are further validated in capturing the accumulated material damage that is developed during cyclic and dynamic loading conditions, through the use of experimental data found in the international literature. The numerical accuracy and robustness of the proposed modeling method [2] is investigated by comparing the numerical results with the experimental data of two beam-column frame joints, a shear wall and a three-storey three-bay RC frame.

2 MATERIAL MODELING

2.1 Concrete Material Modeling and Damage Factor

The proposed numerical model adopted herein is based on the experimental findings of Kotsovos and Newman [3], which were derived from tests on specimens subjected to triaxial loading conditions, through the use of techniques capable of both inducing definable states of stress in the specimens and measuring reliably the deformational response of concrete [4]. Based on the experiment findings [4], the concrete material loses all of its carrying capacity

when the criterion of failure is satisfied, thus the adopted material model assumes that the cracked concrete will behave in a brittle manner. The expression of the strength envelope of concrete that was used during the nonlinear analysis in this research work is provided in Eq. 1 and it's based on the Willam and Warkne [5] formulae.

$$\tau_{0u} = \frac{2\tau_{0c}(\tau_{0c}^2 - \tau_{0e}^2)\cos\theta + \tau_{0c}(2\tau_{0e} - \tau_{0c})\sqrt{4(\tau_{0c}^2 - \tau_{0e}^2)\cos^2\theta + 5\tau_{0e}^2 - 4\tau_{0c}^2\tau_{0e}^2}}{4(\tau_{0c}^2 - \tau_{0e}^2)\cos^2\theta + (2\tau_{0e} - \tau_{0c})^2} \tag{1}$$

The concrete stress-strain relationships are expressed most conveniently by decomposing each state of strain and stress into hydrostatic and deviatoric components describing a realistic behavior of concrete under generalized three-dimensional states of stress. The constitutive relations take the following form:

$$\varepsilon_0 = \varepsilon_{0(h)} + \varepsilon_{0(d)} = (\sigma_0 + \sigma_{id})/(3K_s) \tag{2}$$

$$\gamma_0 = \gamma_{0(d)} = \tau_0/(2G_s) \tag{3}$$

where K_s and G_s are the secant forms of bulk and shear moduli, respectively. The secant forms of bulk, shear modulus and σ_{id} are expressed as functions of the current state [4] take into account the coupling effect of τ_0-$\varepsilon_{0(d)}$ (h and d stand for hydrostatic and deviatoric components, respectively). It must be also noted herein that, the model uses the smeared crack approach for simulating cracking, therefore, the model simulates the geometrical discontinuity by the assumption of displacement continuity and by modifying the material properties along the crack plane. This approach avoids the need of remeshing when cracks open and close during the cyclic analysis.

Furthermore, a new criterion of crack closing which was introduced in [1] is used that defines the crack closure in a numerical manner. The criterion has the following form:

$$\varepsilon_i \leq a \cdot \varepsilon_{cr} \tag{4}$$

where ε_i is the current strain in the i-direction normal to the crack plane and ε_{cr} is the strain that caused the crack formation. Parameter a is a reduction factor described by Eq. 5.

$$a = 1 - \frac{\varepsilon_{cr}}{\varepsilon_{\max}} = \frac{\varepsilon_{\max} - \varepsilon_{cr}}{\varepsilon_{\max}} \tag{5}$$

The maximum strain ε_{max} is determined through the iterative Newton-Raphson procedure. For more details in regards to the closing crack criterion one may refer to [5]. According to the solution strategy and the material modeling of concrete [2], when the criterion of crack-closure is satisfied at a Gauss Point (assuming that this point had prior to that only one crack formation), a part of the stiffness is lost along the crack plane at this Gauss Point to account for the damage accumulation due to the opening and closing of the under study crack. Therefore, the proposed damage factor [2] modifies the constitutive matrix of concrete accordingly to model the stiffness deterioration. The damage factor is denoted as D_C and describes the accumulated energy loss due to the number of times a crack has opened and closed. After a numerical investigation, the proposed damage factor was found to perform in a numerically optimum manner when it takes the form of Eq. 6:

$$D_c = e^{-(1-a)/f_{cc}} = e^{-\left(1-\left(1-\frac{\varepsilon_{cr}}{\varepsilon_{\max}}\right)\right)/f_{cc}} = e^{-\left(\frac{\varepsilon_{cr}}{\varepsilon_{\max}}\right)/f_{cc}} \tag{6}$$

where f_{cc} is the number a crack has closed during the cyclic loading history and it is updated in every iteration for every Gauss Point.

After the crack closure, the stresses are corrected by using the following expression:

$$\sigma^i = \sigma^{i-1} + C' \cdot \Delta\varepsilon^i \tag{7}$$

where *C'* is the modified constitutive matrix of concrete with the damaged material properties across the direction of the closed cracks. The constitutive matrix takes the following form:

$$\boldsymbol{C}_i^{'} = \begin{bmatrix} 0.25\cdot(1-D_c)\cdot(2G_t+\mu) & 0.25\cdot(1-D_c)\cdot\mu & 0.25\cdot(1-D_c)\cdot\mu & 0 & 0 & 0 \\ 0.25\cdot(1-D_c)\cdot\mu & 2G_t+\mu & \mu & 0 & 0 & 0 \\ 0.25\cdot(1-D_c)\cdot\mu & \mu & 2G_t+\mu & 0 & 0 & 0 \\ 0 & 0 & 0 & 0.125\cdot(1-D_c)\cdot\beta\cdot G_t & 0 & 0 \\ 0 & 0 & 0 & 0 & 0.125\cdot(1-D_c)\cdot\beta\cdot G_t & 0 \\ 0 & 0 & 0 & 0 & 0 & 0.125\cdot(1-D_c)\cdot\beta\cdot G_t \end{bmatrix} \tag{8}$$

where β is the concrete shear retention factor. Additionally, the material deterioration that occurs due to the opening and closing of cracks affects the bonding relation between the steel reinforcement and the damaged concrete domain that contains them. In order to take into account this loss of bonding, a modification of the steel stress-strain relation of Menegotto-Pinto [6] was proposed in [2]. Therefore, pinching characteristics that are caused by the loss of bonding between steel reinforcement and its surrounding concrete medium can be taken into account indirectly by reducing the stiffness contribution of the steel reinforcement [2]. In order to numerically establish such a connection, the average of all parameters *a* (Eq. 5) at the 8 Gauss Points within each concrete hexahedral element is computed and used to determine the overall level of damage of each concrete hexahedron found within the concrete mesh. Eq. 9 gives the expression through which the steel damage factor is computed through the use of the damage factor *a*.

$$D_s = \left[1 - a_{Element}\right] \tag{9}$$

where,

$$a_{Element} = \frac{\sum_{1}^{ncr} a_i}{ncr}, \; ncr \text{ is the number of cracked Gauss Points} \tag{10}$$

The material deterioration of the steel reinforcement is computed based on the following proposed formulae:

$$E_s^{'} = (1-D_s)E_s \tag{11}$$

where E_s' is the modified steel modulus of elasticity. As explained in [7], an alternative way of introducing the pinching effect through the stress-strain law of steel reinforcement, is by reducing the parameter *R* of the Menegotto-Pinto [6], which has the following form:

$$R = R_0 - \frac{a_1 \xi}{\alpha_2 + \xi} \tag{12}$$

where ξ is the strain difference between the current asymptote intersection point and the previous load reversal point with maximum or minimum strain, depending on whether the corresponding steel stress at reversal is positive or negative. R_0, a_1 and a_2 were assumed to be 20, 18.5 and 0.15, respectively, in this study. Therefore, by using the same reduction factor the parameter R' is calculated though the following expression:

$$R' = (1 - D_R)R \text{, where } D_R = D_s \tag{13}$$

In this case, the material deterioration is applied when the criterion $\sigma_s \cdot \varepsilon_s < 0$ is satisfied during the nonlinear analysis. This criterion describes the situations when crack closures and re-openings occur, where the pinching phenomena are present. The modified material model is shown in Fig. 1 for different damage levels.

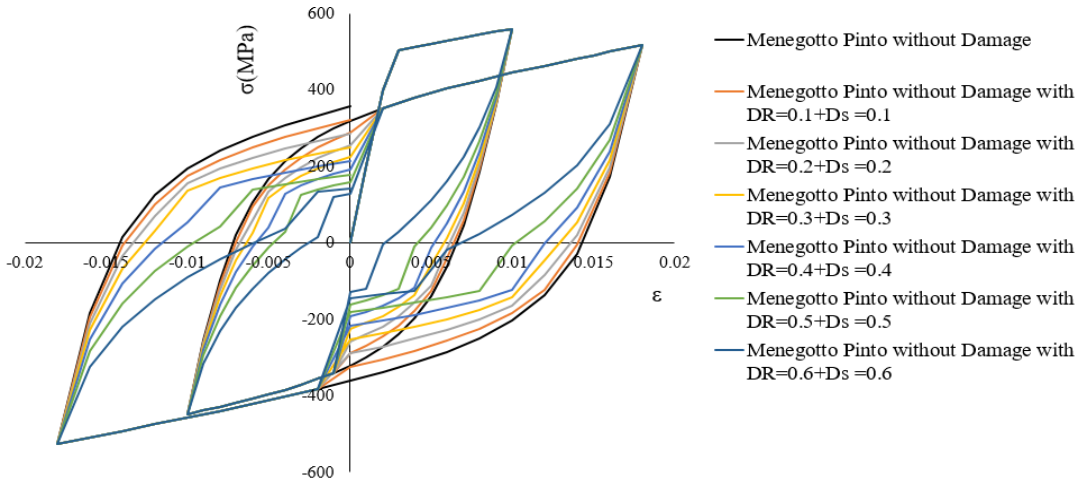

Figure 1: Menegotto-Pinto steel model by taking into account the accumulated damage due to opening/closure of cracks. Different damage levels. [7]

3 NUMERICAL IMPLEMENTATION

3.1 Beam-Column frame joints

Two beam-column joints shown in Fig. 2, were tested by Shiohara and Kusuhara [8] under static cyclic loading. The uniaxial compressive concrete strength was reported to be equal to f_c = 28.3 MPa and the yielding stress of the steel reinforcement was 456 MPa for the 13 mm in diameter rebars found in the beam section. The rebars placed within the column section, were reported to have a 357 MPa yielding stress [8]. The Young modulus of elasticity for the longitudinal reinforcement was reported to be equal to E_S = 176 GPa, where 6 mm stirrup reinforcement had a yielding stress of 326 MPa and a Young modulus of elasticity equal to 151 GPa.

The frame joint was subjected to different cyclic loading sets according to the experiment [8]. The loading history that was numerically applied in this work, is presented in the form of 15 cycles of imposed displacements as shown in Fig. 3 and as it was reported in [8].

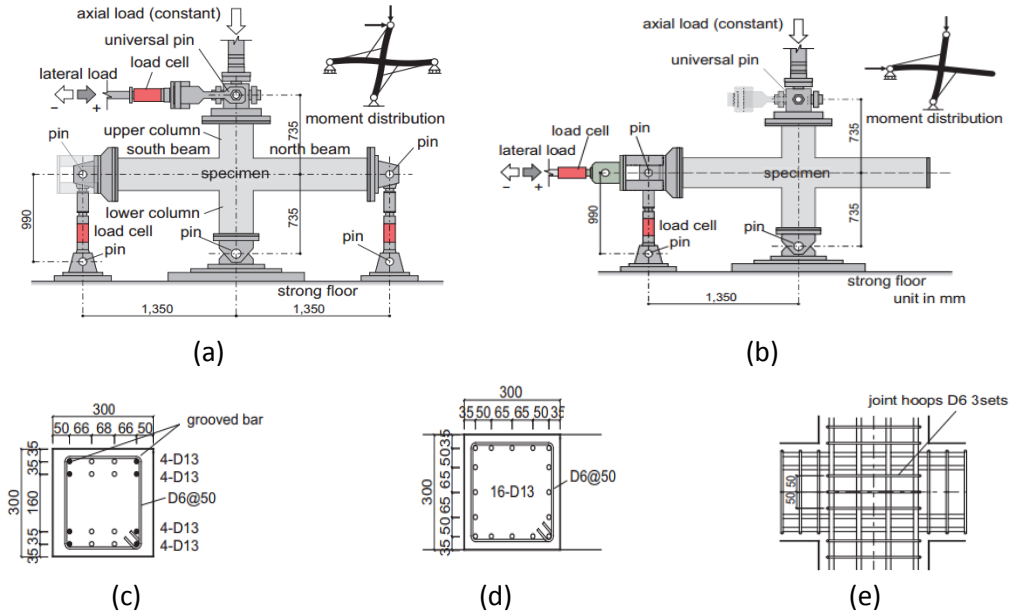

Figure 2: Beam-Column joints. Geometry of (a) A1 and (b) A3 specimens, and reinforcement details of the (c) beam, (d) column and (e) joint section. [8]

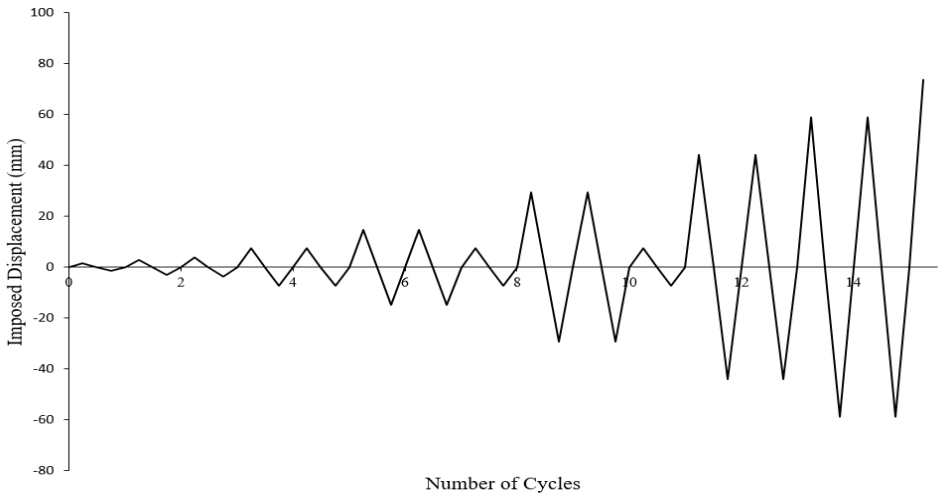

Figure 2: Beam-Column joints. Imposed displacement history.

For the modeling requirements, the concrete domain was discretized with 8-noded hexahedral finite elements and the steel reinforcement was discretized with beam-column finite elements. A total number of 128 concrete (23cm x 15cm x 15cm) and 888 steel Natural Beam-Column Flexibility-Based (NBCFB) finite elements were used to discretize the entire frame joint. Specimen A1 was simulated as an interior beam-column joint, while specimen A3 was developed to simulate the conditions of an exterior corner joint. The boundary conditions of the numerical model can be seen in Fig. 4, where the displacements were imposed at the top section of the column for specimen A1 and at the left edge of the beam for specimen A3 (according to the experimental setup described in [8]). A 216 kN compressive force was applied at the top section of the column for both specimens. Additionally, 8-noded hexahedral finite

elements were used at the support and at the sections where displacements are imposed to simulate the metallic plates, which were placed in order to avoid local failure.

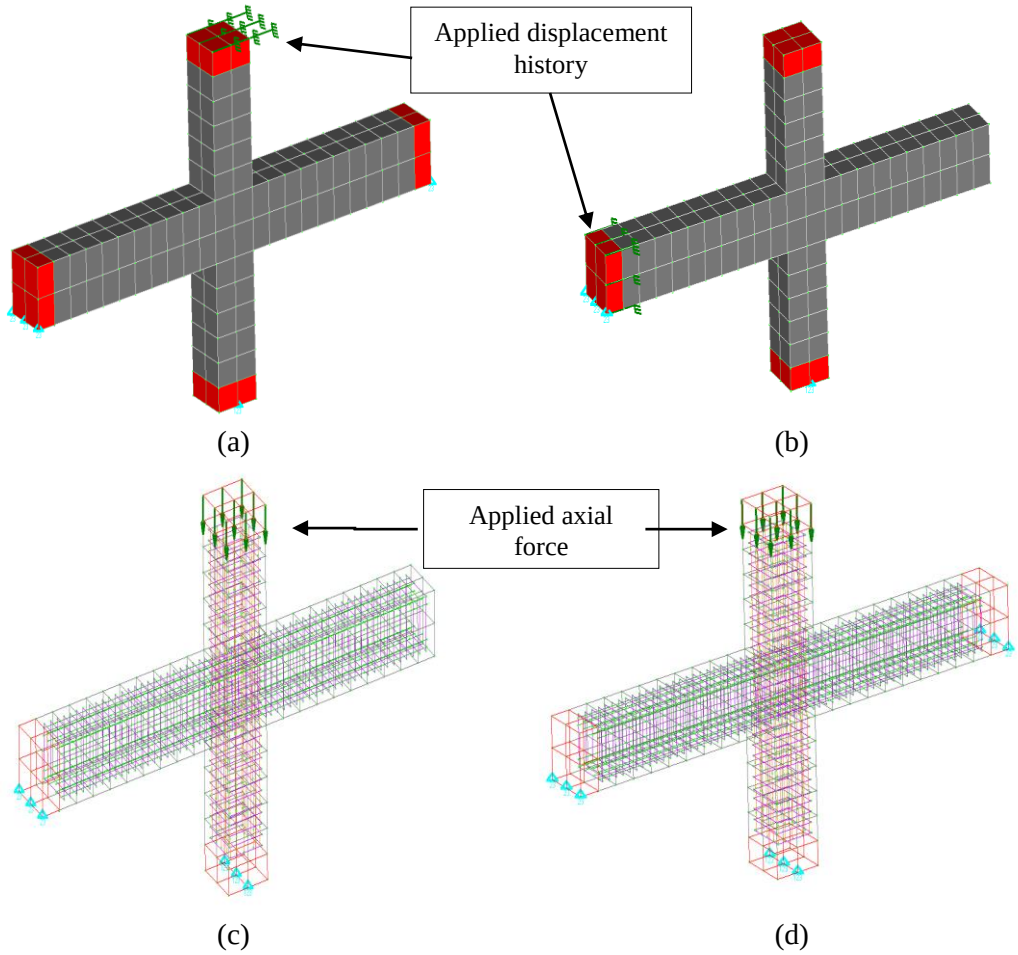

Figure 4: RC beam-column frame joint. Finite element concrete mesh with imposed displacements for specimens a) A1 and (b) A2. Steel reinforcement mesh and applied axial loads for specimens c) A1 and (d) A2.

The numerically computed force-displacement curves are compared with the corresponding experimental data in Fig. 5. As can be seen, the numerical results match very well with the experimental data, where the stiffness and the resulted load-carrying capacity of the specimen were predicted in an accurate manner. Furthermore, the numerical energy dissipation values were found to be close to the experimental ones. Fig. 6 also shows the force-displacement curves and the corresponding hysteretic behavior when the proposed damage factors for concrete and steel reinforcement are being activated and deactivated for the modeling of specimen A1. The numerical results show that the concrete damage factors manage to capture the stiffness and load-capacity degradation, whereas the pinching characteristics are captured through the use of the steel material damage factor (see Fig. 6b).

When modeling the A3 specimen, the pinching effect is observed to be smaller than the experimental one. This is probably attributed to the loss of bond, which resulted during the experimental test (Fig. 5) due to the slippage of the steel reinforcement. Nonetheless, the numerical model manages to capture the hysteretic behavior with an acceptable accuracy.

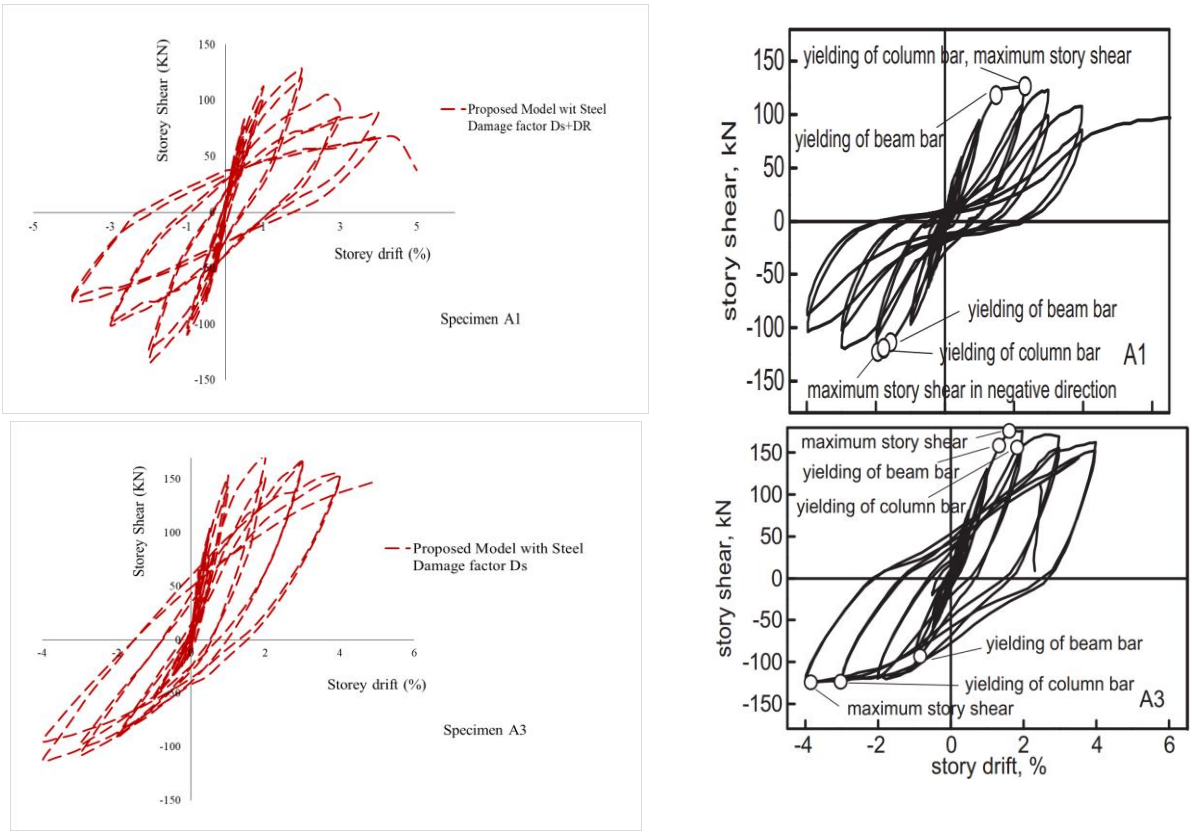

Figure 5: Beam-Column frame joint. Comparison between numerical (Left) and experimental results [8] (Right). Complete force-displacement history for specimens A1 (up) and A3 (down).

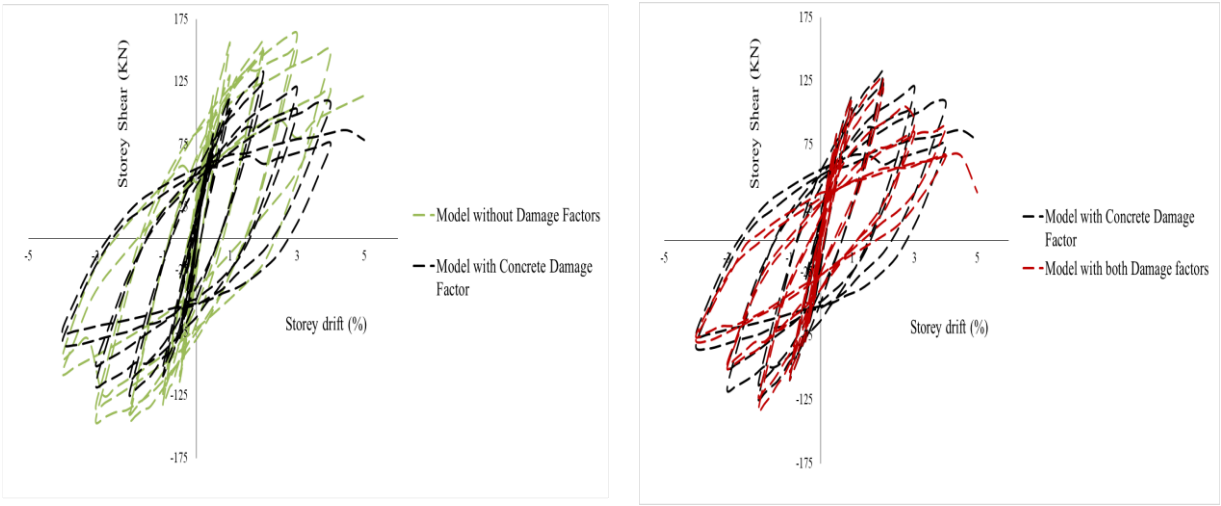

(a) (b)

Figure 6: Beam-Column frame joint. Comparison between numerical results that were obtained by activating and deactivate the two damage factors for specimen A1. Comparison between numerical results when a) Model assumes no damage factors and compared to the model that assumes only for the concrete damage factor. b) Model with concrete damage factor only and compared to the case with both damage factors activated.

Furthermore, as it resulted from the numerical investigation, the hysteretic loops of specimen A3 produce larger hysteretic loops when compared with that of specimen A1, a mechanical behavior that can be easily observed through Figs. 5 and 6. Based on the numerical findings obtained through the analysis of the two specimens, it can be concluded that the use

of both damage factor (D_C, D_S) play an important role in capturing the strength and stiffness deterioration of the RC specimens.

According to the numerically obtained results, Table 1 was developed to compare the numerically predicted maximum (negative and positive) storey shear forces with the corresponding experimental data. The comparison shows that the discrepancy between the numerical and the experimental data is lower than 10%.

Specimen		Maximum Storey Shear		Divergence from Experiment (%)
		Experimental (kN)	Numerical (kN)	
A1	(+)	126.6	127.84	0.98
	(-)	-122.8	-134.12	-9.21
A3	(+)	176.4	171.16	-2.97
	(-)	-124.5	-112.98	9.25

Table 1: Beam-Column frame joint. Comparison of the maximum storey shear between experimental and numerical results.

3.2 RC Shear wall SW4

The RC shear wall investigated by Pilakoutas and Elnashai [9], was also analyzed by using the proposed model. The shear wall was denoted as SW4 and it has a rectangular geometry with a 1.2 m height and a 0.6 m length, where its thickness was reported to be equal to 0.06 m, as showed in Fig. 7. The material properties and reinforcement details are given in Table 2, as they were reported in [9].

Region	Concrete		Horizontal Reinforcement		Vertical Reinforcement		Confining Reinforcement	
	f_c (MPa)	E_c (MPa)	ρ (%)	f_y (MPa)	ρ (%)	f_y (MPa)	ρ (%)	f_y (MPa)
Web	36.9	35240	0.39	545	0.5	545	-	-
Boundary	36.9	35240	0.79	545	6.86	470	0.43	545

Table 2: Material properties and reinforcement ratios of Shear wall SW4

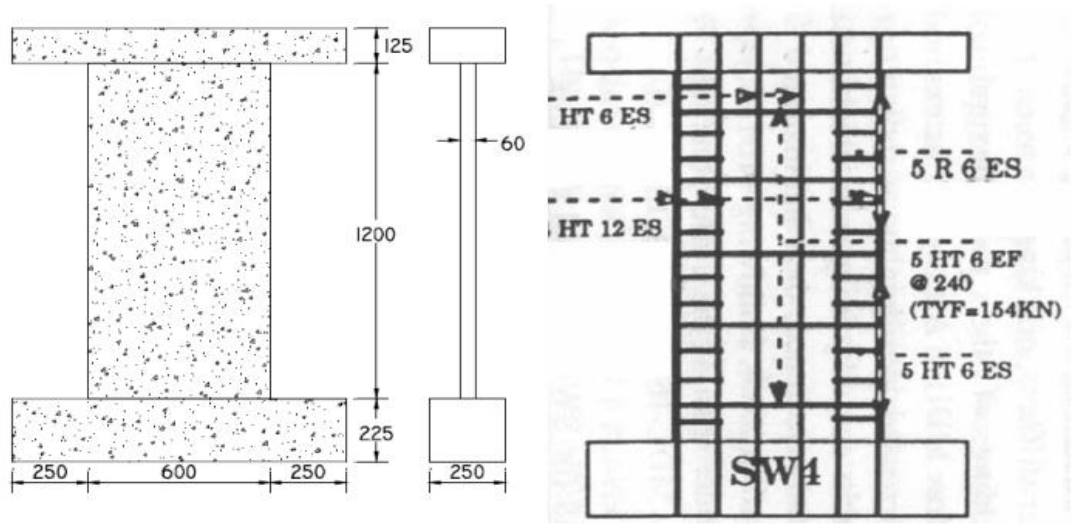

Figure 7: Geometric and reinforcement details of Shear wall SW4 [9].

The shear wall was subjected to different cyclic loading sets according to the experimental setup [9]. The loading history represents extreme conditions experienced during a severe earthquake and it was modeled as shown in Fig. 8. The concrete domain was discretized with 8-noded hexahedral finite elements and the steel reinforcement was discretized with NBCFB elements. A total number of 50 concrete (23cm x 15cm x 15cm) and 250 steel embedded rebar elements were used to discretize the entire shear wall as shown in Fig. 9. Additionally, rigid hexahedral elements were used to simulate the metallic plates near the boundaries in order to avoid local failure (red elements in Fig. 9).

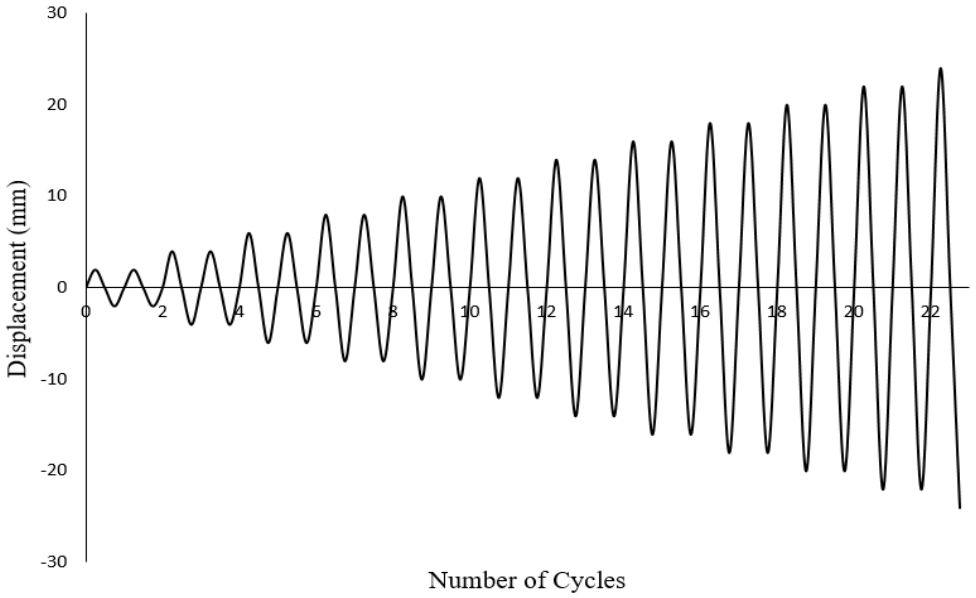

Figure 8: Loading history imposed at the top beam of specimen SW4.

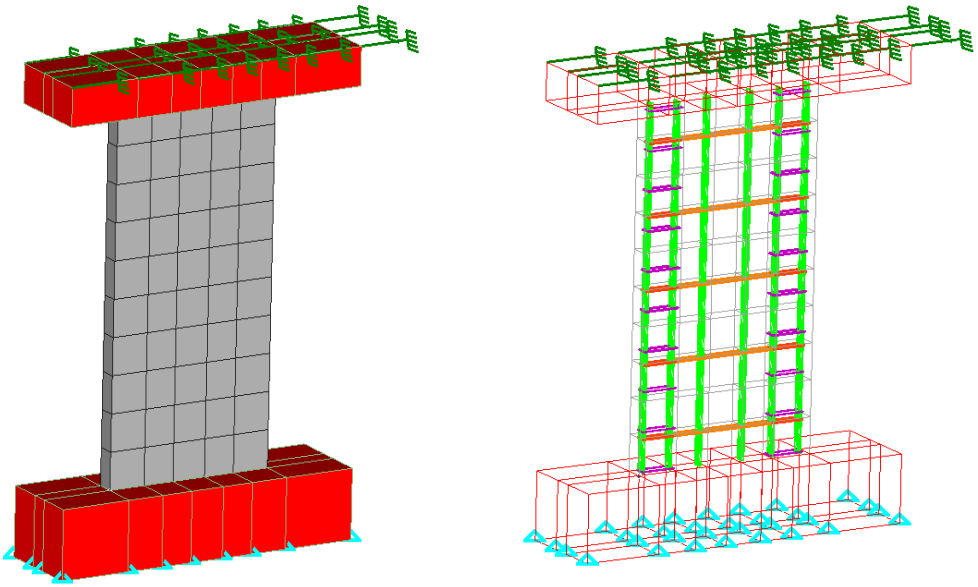

Figure 9: Shear wall SW4. 3D views of the finite element meshes of concrete and embedded rebar elements.

The numerically obtained curves are compared with the corresponding experimental data in Fig. 10. As can be seen, the numerical results match very well with the experimental data,

where the stiffness and the load-carrying capacity of the specimen were predicted in an accurate manner (less than 10% deviation from the experimental data). Furthermore, the numerical energy dissipation of the structure was found to be very close to the experimental one. In addition, the experimental results show a more flexible behavior in terms of structural response without significant pinching effect characteristics. The same mechanical behavior was captured from the numerical results that also did not indicate for any significant pinching behavior.

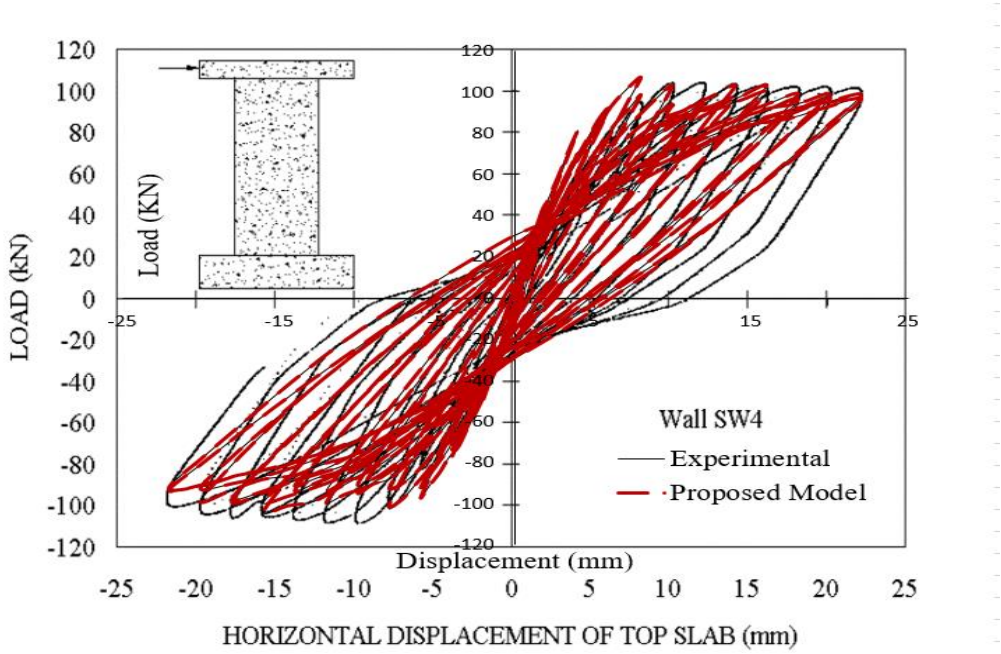

Figure 10: Shear Wall SW4. Comparison between numerical and experimental results in terms of the force-deflection curves.

3.3 Three-storey, Three-bay RC Frame Subjected to High Intensity Ground Motions

A three-storey, three-bay frame was designed, built and tested at the University of California, Berkeley [10] in order to study the collapse behavior of RC frames with light transverse reinforcement. The geometrical and reinforcement details of the specimen can be depicted in Fig. 11. The RC frame was subjected to a dynamic loading test. The cylindrical compressive strength of concrete that was used to construct the RC frame, was equal to f_c = 24.6 MPa, where the yielding stress of the longitudinal steel reinforcement was reported to be equal to f_y = 445 MPa. Additionally, the beam and column ties were 4.8 and 3.2 mm in diameter with a yielding strength of 558 and 655 MPa, respectively.

Two of the columns, as shown in Fig. 11, have been designed according to ACI 318-08 [11] and they were referred to as "ductile" columns with a longitudinal reinforcement ratio of ρ_l = 1.09% and a transverse reinforcement ratio of ρ_t = 1.1% at the end of the column members. The other two columns were referred to as "older type" columns, with longitudinal reinforcement ratio equal to ρ_l = 2.45% and a transverse reinforcement ratio of ρ_t = 0.15%. Furthermore, the beam's transverse reinforcement was also designed according to ACI 318-08 [11], while beam-column joint failure was not expected based on the design provisions of the frame.

Each beam span has been loaded with four packets of lead weights (6.67 kN per packet). The total load (load packets and weight of concrete frame) of the structure produced the equivalent amount of load in a typical office building. Additionally, the resulting gravity axial load on the first-storey interior columns was approximately $0.16A_g f_c$, while the axial load of the exterior loads was approximately of $0.08A_g f_c$ (where A_g is the column gross section area). Therefore, every beam span was considered that it had a uniformly distributed load of 16.67 kN/m, which was the load used to account for the mass contribution within the numerical model developed for the needs of this numerical investigation. The ground motion record from the 1985 Chilean earthquake at Valparaiso (Llolleo Station, Component 100) was chosen for this dynamic test. The motion was scaled up 4.06 times from its original acceleration amplitudes for the dynamic test and it is given in Fig. 12. In addition to that, the ground motion time scale was divided by a factor of $3^{0.5}$ to satisfy the amplitude requirements [10].

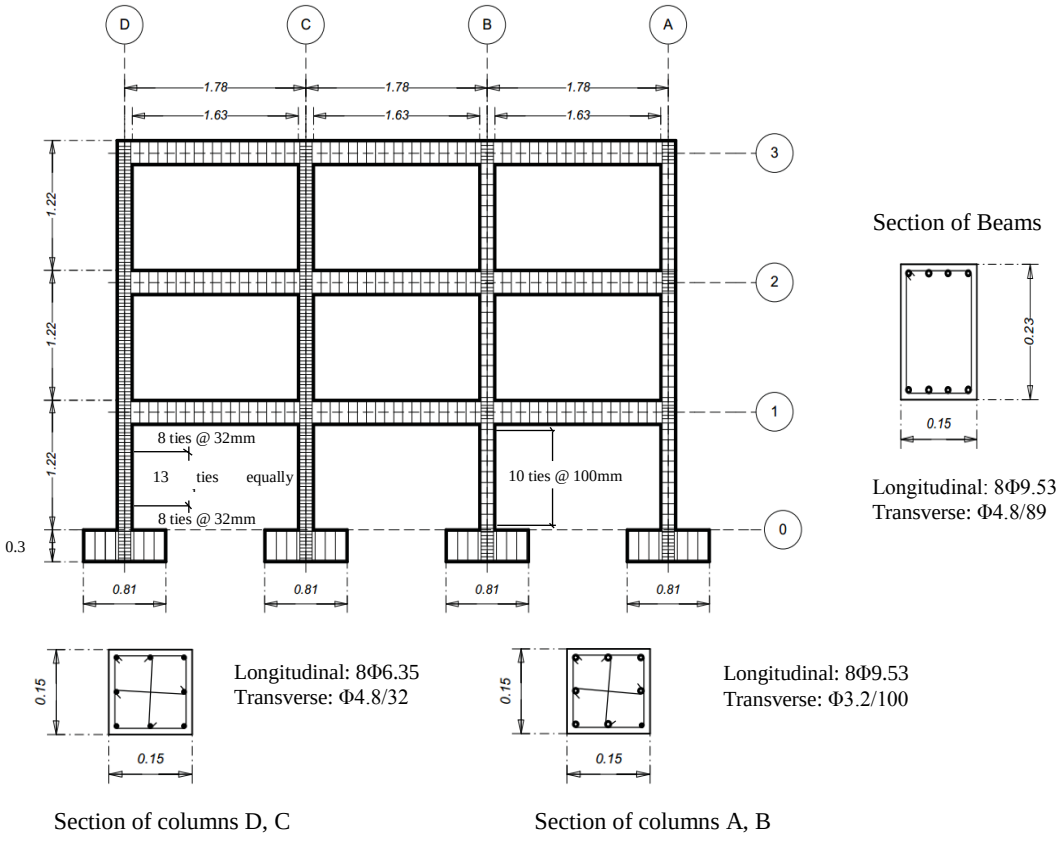

Figure 11: Three-storey, three-bay RC frame. Geometrical and reinforcement details. [10]

For the modeling requirements, the concrete mesh foresaw the use of 336 hexahedral elements and 4,554 steel embedded rebar NBCFB elements were used to model the reinforcement of the specimen, as shown in Fig. 13. Furthermore, 108 hexahedral elements are used (red elements, see Fig. 13) in order to account for the additional mass placed on the structure. In order to account for the exact applied load through the packets, the red hexahedral elements where assigned a mass density that would derive the corresponding load after it was multiplied by its volume. Finally, 60 hexahedral elements (blue elements, see Fig. 13) were used

for the support of the columns so as to simulate the boundary conditions of the specimen and to avoid any local failure at the area where the accelerogram was applied.

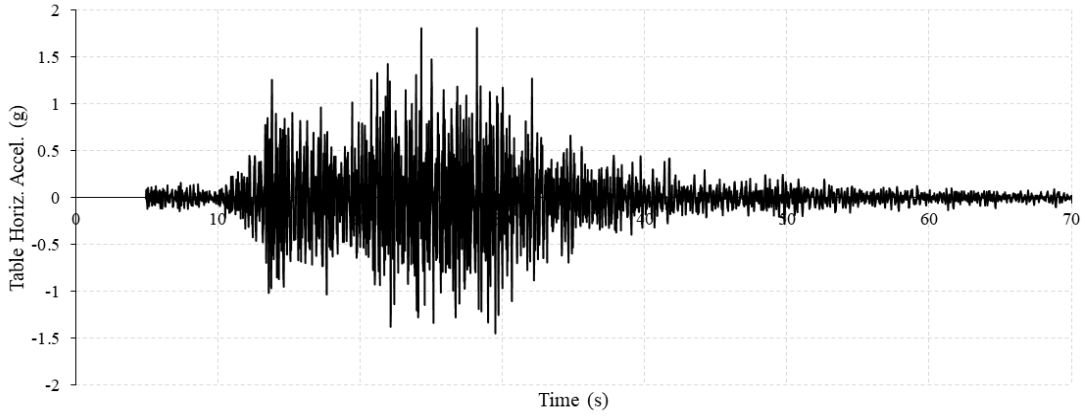

Figure 12: Three-storey, three-bay RC frame. Acceleration history used during the experiment [10].

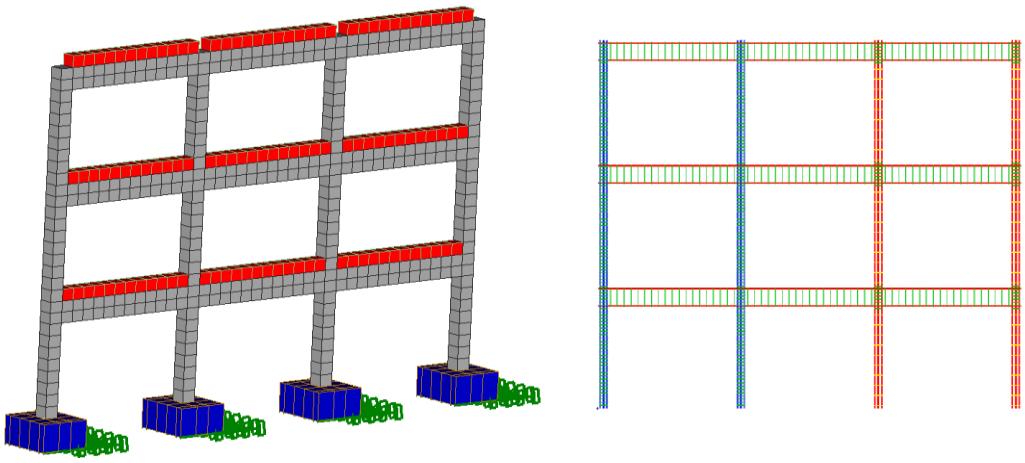

Figure 13: Three-storey, three-bay RC frame. 3D view of the finite element mesh of the (a) 8-noded hexahedral and (b) embedded rebar elements.

The natural periods for the first three modes were compared with the corresponding experimental ones and given herein in Table 3. The comparison shows that the natural periods that derived from the numerical model, were very close to the experimental ones, where the average computed error was equal to 8.7%.

Mode	Experimental period T (s)	Numerical period T (s)	Divergence from experimental (%)
First	0.30	0.30	0
Second	0.10	0.09	10
Third	0.069	0.08	15.94
		Average	8.65

Table 3: Three-storey, three-bay RC frame. Comparison between the numerically and the experimentally derived natural periods.

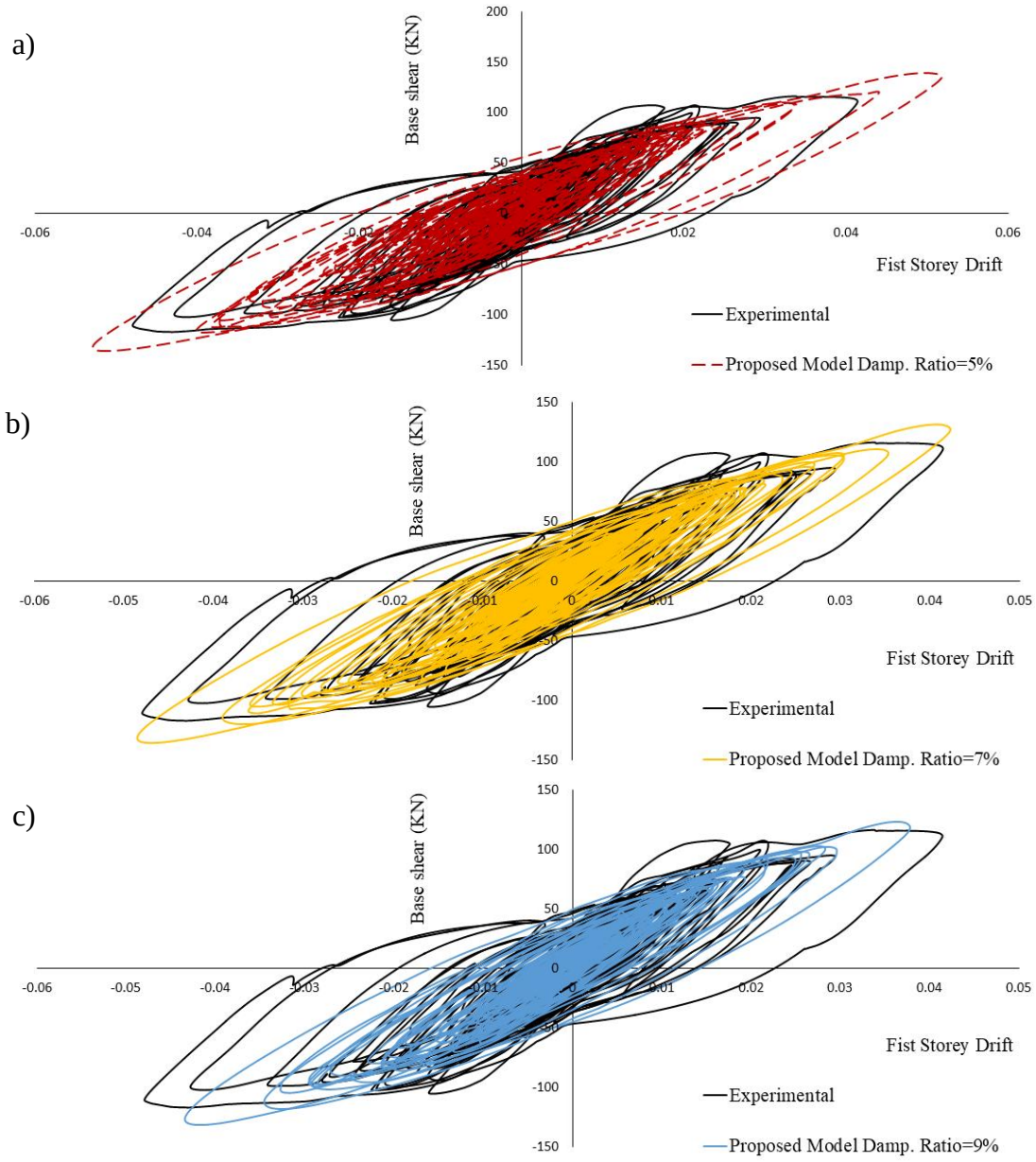

Figure 14: Three-storey, three-bay RC frame. Comparison between the numerical and experimental results of base shear-fist storey drift curves when using damping ratio equal to (a) 5%, (b) 7% and (c) 9%.

Fig. 14 shows the force-displacement curves comparison between the numerical and experimental data. For the needs of this numerical investigation, three different damping ratios were examined (9%, 7% and 5% damping). Based on the analysis of the computed curves, it was found that the two numerical models that adopt damping ratios equal to 7% and 9% produce more accurate results in comparison to the model with a 5% damping ratio. It is also easy to observe that the proposed modeling method manages to capture the overall dynamic response of the specimen, maintaining a good accuracy when compared with the experimental curves. It important to note at this point that, during the experiment, there was a steel frame that was post-tensioned to the shake table on each side of the concrete frame to restrain the out-of-plain movements. This frame could have had an impact on the stiffness of the specimen and on the damping mechanisms that were developed. This effect was not accounted for

during the numerical results and can explain the differences between the curves given in Fig. 14.

The required Newton-Raphson internal iterations per displacement increment are shown in Fig. 15 for the case where the damping ratio was set to 9% (similar results derived when the use of 5% and 7% damping ratios is adopted). It can be easily seen that all the displacement increments require a minimal number of iterations to achieve convergence, regardless the degree of nonlinear behavior of the model. As it can be seen, the required internal iterations per dynamic step during the solution procedure were limited to 1 to 2, underlining the numerical stability of the proposed modeling method [2]. The computational time for the nonlinear solution procedure is given in Table 4, which refers to the solution of 12,125 dynamic time increments. The total required time for solving the nonlinear dynamic problem was 658.5s with an average error of 1.1×10^{-5}. It is important to note herein that, the CPU used to perform all the analyses in this study had a 3.7 GHz computing power.

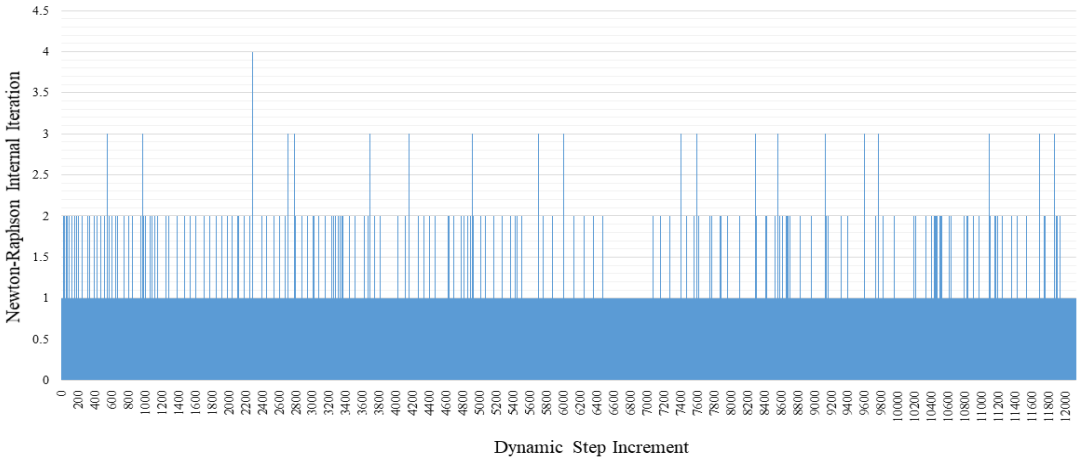

Figure 15: Three-storey, three-bay RC frame. Number of internal iterations per dynamic step increment.

Task	CPU Time (s)
Embedded rebar element mesh generation	0.24
Nonlinear incremental-iterative solution	658.22
Total Time	658.46

Table 4: Three-storey, three-bay RC frame. CPU time for different tasks of the nonlinear analysis.

4 CONCLUSIONS

In this research paper, a proposed 3D constitutive modeling approach is used for the analysis of RC structures that are subjected to limit states static cyclic and dynamic loading conditions. The concrete material constitutive model was found to describe a realistic behavior of concrete under generalized 3D states of stress. Based on the adopted modeling method of concrete, the cracking phenomenon was modeled through the smeared crack approach. The introduction of two damage parameters for concrete and steel reinforcement materials in order to take into account the accumulated damage during the nonlinear analysis was found to pro-

vide the analysis with objectivity and numerical accuracy when dealing with extreme nonlinearities.

Furthermore, the proposed numerical model managed to capture the mechanical behavior of two RC beam-column frame joints, a shear wall and a three-storey three-bay RC frame that was tested under extreme dynamic loading conditions. This validation study is an extension on the research work presented in [2] that reported similar findings.

Based on the numerical findings of the research work presented herein, for the case of the RC beam-column joints, the damage parameter for steel reinforcement was found to be able to take into account for the loss of bonding within the damaged concrete areas, where it manages to partially capture the pinching characteristics observed within the experimental hysteretic curves. For extreme pinching modeling through the use of the proposed modeling approach, one may refer to [7].

Finally, the thee-storey RC frame specimen was modeled for both modal and nonlinear dynamic analysis. According to the parametric investigation, the first three natural modes were captured with an overall deviation from the experimental data equal to 8.7%, a finding that highlights the ability of the developed algorithm in capturing the modes of a real structural system. Finally, the dynamic analysis of the RC frame that was designed to exhibit a brittle behavior was performed successfully through the use of different damping rations. The ability of the proposed modeling method in capturing the nonlinear dynamic response of the RC frame through the use of the exact material properties (as they were reported within the report [10]) demonstrates its computational superiority, indicating that it is a powerful tool when it comes to the modeling of RC structures.

REFERENCES

[1] Mourlas, C., Papadrakakis, M., Markou, G. *A computationally efficient model for the cyclic behavior of reinforced concrete structural members*. Engineering Structures, Vol. **141**, pp. 97–125, 2017.

[2] Mourlas, C., Markou, G., Papadrakakis, M. *Accurate and computationally efficient nonlinear static and dynamic analysis of reinforced concrete structures considering damage factors*. Engineering Structures, Vol. 178, pp. 258–85, 2019.

[3] Kotsovos, M.D., Newman J.B. *Behavior of Concrete Under Multiaxial Stress*. ACI Journal Proceedings, Vol. **74**(9), pp. 213–23, 1977.

[4] Kotsovos, M.D., Pavlovic, M. *Structural concrete : finite-element analysis for limit-state design.* T. Telford; 1995.

[5] Willam, K., Warnke, E.P. *Constitutive model for the triaxial behavior of concrete*. Seminar on concrete structures subjected to triaxial stresses, Instituto Sperimentale Modeli e Strutture, Bergamo, Paper III-1., 1974.

[6] Menegotto, M., Pinto, P.E. *Method of analysis for cyclically loaded reinforced concrete plane frames including changes in geometry and non-elastic behavior of elements under combined normal force and bending*. Proceedings, IABSE Symposium on Resistance and Ultimate Deformability of Structures Acted on by Well Defined Repeated Loads, Lisbon, Portugal, 15–22., 1973.

[7] Markou, G., Mourlas, C., Garcia, R., Pilakoutas, K., Papadrakakis, M., “Cyclic

Nonlinear Modeling of Severely Damaged and Retrofitted Reinforced Concrete Structures", COMPDYN 2019, 7th International Conference on Computational Methods in Structural Dynamics and Earthquake Engineering, 24-26 June 2019, Crete, Greece.

[8] Shiohara, H., Kusuhara, F. *Benchmark Test for Validation of Mathematical Models for Nonlinear and Cyclic Behaviour of R/C Beam–Column Joints.* Department of Architecture, School of Engineering, University of Tokyo: 2006.

[9] Elnashai, A.S., Pilakoutas, K., Ambraseys, N.N. *Experimental behaviour of reinforced concrete walls under earthquake loading.* Earthquake Engineering & Structural Dynamics, Vol. **19**(3), pp. 389–407, 1990.

[10] Ghannoum, W.M., Moehle, J.P. *Experimental Collapse of a Lightly Reinforced Concrete Frame Subjected to High Intensity Ground Motions*. 14th World Conference on Earthquake Engineering, vol. 12-01-0052, Beijing, China: 2008, p. 12–7.

[11] ACI Committee 318. *Building Code Requirements for Structural Concrete (ACI 318-95) and Commentary*. American Concrete Institute, Farmington Hills, MI: 1995.